



1 Impacts on cloud radiative effects induced by coexisting aerosols 2 converted from international shipping and maritime DMS emissions

3 Qinjian Jin¹, Benjamin S. Grandey², Daniel Rothenberg¹, Alexander Avramov^{1†}, Chien Wang^{1,2}

4 ¹Center for Global Change Science, Massachusetts Institute of Technology, Cambridge, Massachusetts, USA.

5 ²Center for Environmental Sensing and Modelling, Singapore–MIT Alliance for Research and Technology, Singapore.

6 † Now at Department of Environmental Science, Emory University, Atlanta, Georgia, USA.

7 Correspondence to: Qinjian Jin (jqj@mit.edu)

8 **Abstract.** International shipping emissions (ISE), particularly sulfur dioxide, can influence the global radiation budget by
9 interacting with clouds and radiation after being oxidized into sulfate aerosols. A better understanding of the uncertainties in
10 estimating the cloud radiative effect (CRE) of ISE is of great importance in climate science. Many international shipping tracks
11 cover oceans with substantial natural dimethyl sulfide (DMS) emissions. The interplay between these two major aerosol sources
12 on cloud radiative effects over vast oceanic regions with relatively low aerosol concentration is an intriguing yet poorly
13 addressed issue confounding estimation of the cloud radiative effects of ISE. Using an Earth system model including two aerosol
14 modules with different aerosol mixing configurations, we derive a significant global net CRE of ISE (-0.153 W m^{-2} with $p=0.01$
15 and standard error of 0.004 W m^{-2}) when using emissions consistent with current ship emission regulations. This global net CRE
16 would become much weaker and actually insignificant (-0.001 W m^{-2} with $p=0.98$ and standard error of 0.007 W m^{-2}) if a more
17 stringent regulation were adopted. We then reveal that the ISE-induced CRE would achieve a significant enhancement when
18 lower DMS emission is prescribed in the simulations, owing to the sub-linear relationship between aerosol concentration and
19 cloud response. In addition, this study also demonstrates that the representation of certain aerosol processes, such as mixing
20 states, can influence the magnitude and pattern of the ISE-induced CRE. These findings suggest a re-evaluation of the ISE-
21 induced CRE with consideration of DMS variability.

22 1 Introduction

23 Marine stratiform clouds have a strong cooling effect on the climate system. They cover about 30% of the global ocean
24 surface (Warren et al., 1988), and can reflect more solar radiation back to space than the dark ocean surface at cloud-free
25 conditions. On the other hand, low-altitude marine stratiform clouds form and develop near to the ocean surface (only several
26 degrees cooler than ocean surface) and thus have limited impacts on the longwave radiation balance (Klein and Hartmann, 1993).
27 Therefore, the annual-mean net radiative effect of cloud at the top of the atmosphere (TOA) is negative (i.e., cooling) and can be
28 up to -20 W m^{-2} on the global scale (Boucher et al., 2013). Consequently, even a few percent change in marine stratocumulus
29 cloud cover can double or offset the anthropogenic global warming due to greenhouse gases.

30 Sulfate aerosols are efficient cloud condensation nuclei and control the formation of marine clouds and their micro- and
31 macro-physical properties (McCoy et al., 2015). The international shipping-emitted sulfur dioxide from combustion of heavy
32 fossil oil (Figure 1) can be oxidized to sulfate aerosols that can increase cloud droplet number concentrations, cloud liquid water
33 path, and planetary albedo, resulting in more solar radiation being reflected back to space, exerting a cooling effect on the
34 climate system (Capaldo et al., 1999; Devasthale et al., 2006; Lauer et al., 2007; Lauer et al., 2009). Although international
35 shipping emissions (ISE) contribute only about 5% (5.6 Tg S yr^{-1}) to the total anthropogenic sulfur emissions (Corbett and
36 Koehler, 2003; Endresen et al., 2005; Klimont et al., 2013), they dominate the sulfur concentration across much of the ocean,



37 such as the North Pacific Ocean (NPO) and the North Atlantic Ocean (NAO), as shown in Figure 2. Therefore, the radiative
38 impact of the ISE via perturbing marine stratocumulus clouds could be large—especially because marine stratocumulus clouds
39 are often collocated with busy shipping lanes (Neubauer et al., 2014).

40 Nevertheless, the estimated global annual mean of the ISE-induced net cloud radiative effect (CRE) at TOA has large
41 uncertainties due to the complication in simulating clouds and aerosol–cloud interactions, ranging from -0.60 to -0.07 W m^{-2}
42 (Capaldo et al., 1999; Lauer et al., 2007; Eyring et al., 2010; Righi et al., 2011; Peters et al., 2012; Partanen et al., 2013).
43 Compared with net CRE, the net direct radiative effect (DRE) of shipping emissions is much weaker, with a magnitude of only
44 -0.08 to -0.01 W m^{-2} , approximately one tenth of the former (Endresen et al., 2003; Schreier et al., 2007; Eyring et al., 2010).

45 Besides shipping-emitted sulfur compounds, oceanic phytoplankton-derived dimethyl sulfide (DMS) is another
46 significant component in the atmospheric sulfur cycle over oceans (Grandey and Wang, 2015; Mahajan et al., 2015; McCoy et
47 al., 2015; Tesdal et al., 2016). DMS can be oxidized by hydroxyl radical or nitrate radical to produce sulfur dioxide and finally
48 converted to sulfate aerosols (Boucher et al., 2003). The global total DMS emission is estimated to range from 8 to 51 Tg S yr^{-1}
49 based on model simulation (Quinn et al., 1993; Dentener et al., 2006); this uncertainty range is itself substantially larger than the
50 total sulfur emissions from shipping. The global annual mean of the DMS-induced net CRE at TOA is from -2.03 to -1.49 W m^{-2}
51 m^{-2} determined by DMS climatology (Gunson et al., 2006; Thomas et al., 2010; Mahajan et al., 2015).

52 Most of the aforementioned studies addressed separately the impacts on CRE of shipping and DMS emissions, largely
53 ignoring the potential nonlinearity in the response of cloud radiative effects to aerosol variations when these sulfate aerosols
54 from two different sources often collocate in the relatively clean marine atmosphere, such as NPO and NAO (Figure 1). The
55 nonlinearity between DMS emission and the associated CRE was studied previously without taking into account the shipping
56 emissions (Pandis et al., 1994; Russell et al., 1994; Gunson et al., 2006; Thomas et al., 2011). Here, to evaluate the CRE induced
57 by both ISE and DMS emissions with a consideration of their interactions, we selected three regions for detailed analysis: the
58 NPO and NAO where the ISE dominate the concentrations of sulfur dioxide and sulfate aerosols, and the Southern Ocean where
59 DMS is the dominant source (Figure 2).

60 This study employs an Earth system model including an interactive aerosol model that simultaneously resolves both
61 external and internal mixtures of sulfate, black carbon, and organic carbon aerosols. Aerosol mixing in this way can resolve
62 aerosol activation process more realistically than either mixing all aerosol species internally or ignoring any mixing at all. By
63 comparing the results with the default aerosol scheme that ignores above mixing processes, we also quantify the impacts of
64 various assumptions of aerosol mixing states on estimates of the CRE of ISE and DMS emissions. We further quantify the ISE-
65 induced CRE based on various regulations of the International Maritime Organization (IMO) on the fuel sulfur content.
66 Therefore, our findings have important implications for policy makers and future estimates of CRE induced by both ISE and
67 DMS emissions.

68 2 Methods

69 2.1 Climate model

70 The Community Earth System Model version 1.2.2 (CESM1.2.2) is configured with the Community Atmosphere Model
71 version 5.3 (CAM5.3). CAM5.3 includes a modal aerosol model with an option of 3 or 7 lognormal distributions of aerosol size
72 (MAM3 or MAM7). In this study, a new modal aerosol model—the two-Moment, Multi-Modal, Mixing-state resolving Aerosol
73 model for Research of Climate (MARC; version 1.0.3 here) (Kim et al., 2008; Kim et al., 2014; Rothenberg and Wang, 2016;
74 Rothenberg et al., 2017; Rothenberg and Wang, 2017; Grandey et al., 2018) is introduced and used to diagnose both the DRE



75 and CRE of ISE. The details of MARC are described in the following section. Aerosol DRE are represented by coupling between
76 aerosols and radiation. Aerosol CRE are included by activating aerosols to work as cloud condensation nuclei and ice nuclei in
77 the stratiform clouds (Morrison and Gettelman, 2008; Gettelman et al., 2010). Parameterization of aerosol activation is based on
78 particle size and hygroscopicity of aerosols. Similar to other climate models, CAM5 does not include aerosol's influence on
79 convective clouds.

80 2.2 MAM3

81 The default aerosol scheme in CESM 1.2.2, MAM3, has three modes, each with a lognormal size distribution: Aitken,
82 accumulation, and coarse. Various aerosol species are internally mixed within each mode. Aitken mode is a mixture of sulfate,
83 secondary organic carbon and sea salt; accumulation mode is mixture of sulfate, black carbon, primary organic carbon,
84 secondary organic carbon, dust, and sea salt; coarse mode is a mixture of dust, sea salt, and sulfate (Liu et al., 2012).

85 2.3 MARC

86 MARC uses seven modes with different lognormal size distribution to represent the population of sulfate and
87 carbonaceous aerosols: three modes for sulfate (nucleation or NUC, Aitken or AIT, and accumulation or ACC), one each for
88 pure black carbon (BC) and pure organic carbon (OC), one mixture of BC–sulfate in core-shell structure (MBS), and one mixture
89 of OC–sulfate (internal mixture; MOS). MARC predicts total particle mass and number concentrations while assuming the
90 standard deviation within each of the seven modes to define at any given time the lognormal distribution of particle size. In
91 addition, carbonaceous mass concentrations inside MBS and MOS are also predicted to allow the mass ratios between sulfate
92 and carbonaceous compositions evolve over time, changing the optical and chemical properties of the mixed aerosols. The
93 emissions of mineral dust and sea salt that MARC uses are calculated by the land surface model and atmosphere model,
94 respectively (Mahowald et al., 2006; Albani et al., 2014; Scanza et al., 2015). Mineral dust and sea salt are each represented by
95 four bins with fixed sizes in MARC. For details of MARC aerosol mode size distribution and chemical parameters, please refer
96 to Rothenberg et al. (2017).

97 2.4 Radiation diagnostics

98 In the diagnostic mode of CESM-MARC, the DRE are diagnosed by calling the radiation scheme three times in each
99 radiation time step. The first call does not include any aerosols. The second call includes only mineral dust and sea salt aerosols.
100 The third call includes all aerosols. The first and third call are diagnostic while the second call is prognostic. Therefore, DRE of
101 only dust and sea salt aerosols are prognostic while all other aerosols including ISE are diagnostic. In the complimentary MAM3
102 simulations, the first radiation call (prognostic) includes all aerosols while the second call (diagnostic) excludes all aerosols. In
103 this way, the DRE and CRE of ISE can be isolated and evaluated separately. Note that all radiative effects are calculated at TOA.

104 2.5 Experimental design

105 Three groups of simulations are designed to evaluate: (a) the DRE and CRE of ISE, and (b) the sensitivity of the ISE-
106 induced CRE to both DMS emissions and aerosol mixing assumptions. CAM5 was run at a horizontal resolution of $1.875^{\circ} \times 2.5^{\circ}$
107 and 30 vertical layers with sea surface temperature (SST), sea ice, greenhouse gas concentrations prescribed at the level of year
108 2000. The aerosol emissions in year-2000 were used except for modified shipping and DMS emissions. The DMS emission is
109 prescribed with a global annual average of $18.2 \text{ Tg S yr}^{-1}$ in DMS reference simulations (Dentener et al., 2006). Each simulation
110 runs for 32 years driven by 12-month cyclic climatological sea surface temperature, with the first 2 years discarded as spin up.



111 Since the observed SST was used, a 2-year period of spin up should be enough for aerosol concentrations and other model
112 components to reach an equilibrium state (e.g., Righi et al., 2011).

113 The first group uses CESM-MARC and includes four simulations, which share the same DMS reference emissions
114 (*DMSRef*) while differing in four various ISE of sulfur compounds (sulfur dioxide and sulfate) (Table 1). *ShipZero_DMSRef*
115 simulation is integrated excluding all aerosol and aerosol precursor emissions from ISE, i.e., sulfur dioxide, sulfate aerosol,
116 organic carbon aerosol, and black carbon aerosol. The other three simulations—*ShipLow_DMSRef*, *ShipRef_DMSRef*, and
117 *ShipHigh_DMSRef*—include the standard emissions of carbonaceous aerosols (e.g., BC and OC) while use three various
118 emission scenarios of sulfur compounds from ISE. The three emission scenarios are based on the assumptions of sulfur content
119 of the heavy fuel oils for ocean-going ships. Currently, the average sulfur content is 2.7% (Corbett and Koehler, 2003; Endresen
120 et al., 2005), which is equivalent to about 5.6 Tg S year⁻¹, referred to as *ShipRef*. On the other hand, as of 2013 the high sulfur
121 fuel oil that has 3.5% sulfur content continued to be permitted outside the Emission Control Areas (Lauer et al., 2009; Winebrake
122 et al., 2009), referred to as *ShipHigh*. However, the IMO has planned to lower the sulfur content to 0.5% outside the Emission
123 Control Areas (Corbett et al., 2007; Winebrake et al., 2009; Notteboom, 2010; International Maritime Organization, 2016) after
124 2020, referred to as *ShipLow*. In *ShipLow* and *ShipHigh*, the total global sulfur shipping emissions are 1.0 and 7.2 Tg S year⁻¹,
125 respectively. The differences between these three and the zero shipping emission scenarios represent how various regulations on
126 marine fuel influence the ISE-induced CRE.

127 The second group also uses CESM-MARC and is comprised of three pairs of simulations: (*ShipRef_DMSZero*,
128 *ShipZero_DMSZero*), (*ShipRef_DMSLow*, *ShipZero_DMSLow*), and (*ShipRef_DMSRef*, *ShipZero_DMSRef*). The annual
129 emission of DMS is 18.2 Tg S year⁻¹ in the *DMSRef* simulations (Dentener et al., 2006; Liu et al., 2012), and half of that in the
130 *DMSLow* simulations. DMS emission is excluded in the *DMSZero* simulations. Each pair of the simulations include *ShipZero*
131 and *ShipRef*, the difference of which represents the ISE-induced impacts. The purposes of the *DMSZero* and *DMSLow*
132 simulations are to quantify the sensitivities of the ISE-induced CRE (i.e., the difference of CRE in each pair of simulations) to
133 DMS emission and the associated large uncertainty in DMS emission, respectively (Quinn et al., 1993; Dentener et al., 2006).
134 DMS emission in the *DMSLow* simulation is 9.1 Tg S year⁻¹, which is close to the lower boundary of DMS emission estimates,
135 i.e., 8 Tg S year⁻¹ (Quinn et al., 1993). Such sensitivities are examined by calculating the differences among the three pairs of
136 DMS simulations.

137 The third group is the same as the second, but using the default MAM3 aerosol module of CAM5.3 in CESM. The
138 purpose for designing the third group is to cross-validate the simulated DMS impacts on the ISE-induced CRE in the second
139 group. One bonus of the third group is to quantify the impacts of using different aerosol modules with different aerosol mixing
140 states on the simulated results. The anthropogenic emissions for MARC are slightly different from those for MAM3. All of the
141 experiments are summarized in Table 1.

142 3 Results

143 3.1 DRE of ISE

144 The all-sky DRE of various aerosol species from ISE is diagnosed as the difference between *ShipRef_DMSRef* and
145 *ShipZero_DMSRef* and shown in Figure 3. The total ISE can cause a global negative (cooling) DRE of -23.5 mW m⁻², with the
146 strongest negative (cooling) DRE in the areas with intense shipping tracks, such as mid-latitude areas in the Pacific Ocean and
147 Atlantic Ocean, South China Sea, North Indian Ocean, and the Red Sea. The sulfate aerosols in the accumulation mode (i.e.,
148 ACC) contribute 89% to the global total DRE, followed by MOS aerosols with a contribution of 22%. Note that OC and MBS



149 has a counteracting warming effect (Remember that all gas-phase and aerosol emissions from shipping have been removed in
150 ShipZero scenarios). The contributions of other aerosol species are very limited and their magnitudes are smaller than 6%. The
151 magnitude of the total cooling effect is within the range from -50 to -10 mW m^{-2} estimated in previous studies (Endresen et al.,
152 2003; Schreier et al., 2007). The meridional variations of global zonally-averaged total DRE show that the DRE has the strongest
153 cooling effect of -80 mW m^{-2} between 30°N and 40°N and becomes weaker towards both polar regions and can be ignored
154 beyond 45°S and 60°N . The all-sky DRE of total aerosols in ShipLow_DMSRef and ShipHigh_DMSRef have similar patterns to
155 those in ShipRef_DMSRef and have magnitudes of $+1.0$ and -33.0 mW m^{-2} , respectively. All of the calculated global DRE
156 values except for BC are confident at the 90% level.

157 3.2 CRE of ISE under various shipping emission regulations

158 The CRE of ISE is much stronger than the DRE and shows different spatial patterns under various shipping emission
159 regulations (Figure 4). At the reference level of shipping emissions (*ShipRef_DMSRef*), significant cooling CRE in SW is
160 simulated in areas of intense shipping tracks, such as the mid-latitude Pacific Ocean and the Baffin Bay between Canada and
161 Greenland, with a global average of -0.218 W m^{-2} . The LW CRE shows positive values in some small areas of high latitude,
162 with a global average of $+0.065$ W m^{-2} . Consequently, the global net CRE (SW+LW) is -0.153 W m^{-2} with a similar spatial
163 pattern to that of SW. At the high level of shipping emissions (*ShipHigh_DMSRef*), the CRE changes to -0.253 , $+0.073$, -0.179
164 W m^{-2} for SW, LW, and net, respectively; more areas show significant changes than in *ShipRef_DMSRef*. Note that all of the
165 above values are statistically significant above the 90% confidence level. However, at the low level of shipping emissions
166 (*ShipLow_DMSRef*), fewer areas demonstrate significant changes than in *ShipRef_DMSRef* and *ShipHigh_DMSRef* and the
167 global averages of the CRE are not significant at the 90% confidence level for SW and net. These results indicate that more
168 stringent shipping emission regulation on sulfur content proposed by the IMO to be applied after 2020 could effectively reduce
169 or even largely eliminate the net CRE induced by ISE.

170 Further analyses demonstrate that the changes in CRE are caused by perturbations in both cloud water path (CWP;
171 Figure S1) and column-integrated cloud droplet number concentrations (CDNC; Figure 5) induced by ISE. Figure S1
172 demonstrates significant increases in total CWP mainly over the NPO and NAO at the reference and high levels of ISE. The
173 increases in total CWP is largely (87%) attributed to liquid CWP with the remaining contribution (13%) from ice CWP at the
174 reference shipping emission level. Such increases in CWP could reflect more solar radiation to space and thus cause a cooling
175 radiative effect at TOA, as shown in Figure 4. Note that very limited areas in North Pacific Ocean show significant increases in
176 ice CWP, indicating that a small portion of surface shipping emissions could be vertically transported to very high altitude and
177 form ice cloud. At the high level of shipping emissions, a larger increase in CWP is simulated, which is consistent with the
178 cooler radiative effects. However, no significant changes are simulated in total, ice, or liquid CWP at the low level of shipping
179 emissions. Associated with increases in CWP, the column-integrated cloud droplet number concentration (CDNC) also illustrates
180 significant increases at all levels of shipping emission (Figure 5), which collocate with increases in CWP (Figure S1) and
181 decrease in CRE (Figure 4) over the NPO and NAO. The sulfate aerosols from shipping emissions are highly efficient cloud
182 condensation nuclei (CCN) and thus can increase the CDNC. Note that cloud area fraction does not demonstrate any significant
183 changes due to shipping emissions (not shown).

184 3.3 CRE of ISE under various DMS emissions

185 The biogenic emissions of DMS over oceans can be oxidized to sulfates and compete against shipping emitted sulfates
186 for CCN and thus could influence the ISE-induced CRE. We find that the shipping emission-induced CRE exhibits significantly



187 different patterns and global averages at different emission levels of DMS (Figure 6). With DMS emissions ranging from the
188 reference level to low and zero levels, the magnitude of the ISE-induced negative CRE at SW increases from 0.218 to 0.457 and
189 2.435 W m^{-2} on global scale, respectively; significant negative CRE is simulated over more areas in the SO. For CRE at LW,
190 more areas with significant warming are seen in the SO, NPO, and NAO, with the global averages change from +0.065 to +0.073
191 and $+0.253 \text{ W m}^{-2}$ when DMS emissions changes from the reference to low and zero levels, respectively. For net CRE, it shares
192 the similar features with those at SW, but with smaller magnitudes.

193 The DMS emissions influence the ISE-induced CRE by perturbing the ISE-induced changes in CWP and column-
194 integrated CDNC (Figures S2 and 7). The shipping emission-induced changes in the total and liquid CWP increase as DMS
195 emission decreases, particularly over the SO, the NPO, and the NAO, while no significant changes are simulated in the ice CWP.
196 The increased CWP is closely associated with the increases in the column-integrated CDNC, which changes from $0.305 \times 10^9 \text{ m}^{-2}$
197 to $0.476 \times 10^9 \text{ m}^{-2}$ and $0.999 \times 10^9 \text{ m}^{-2}$ on global scale as DMS emission decreases. The most prominent increases in CDNC are
198 seen in the SO, NPO, and NAO. These results suggest important roles of DMS emissions playing in modulating the ISE-induced
199 changes in cloud properties and radiation. Note that cloud area fraction does not illustrate any significant change (not shown).

200 As demonstrated in the above analysis, the impacts of DMS emissions on cloud response to shipping emissions are the
201 most prominent over the SO, the NPO, and the NAO, so further analysis are performed over these three regions. Figure 8 shows
202 cloud responses to shipping emission at different DMS emission levels over the three oceanic regions. Generally, cloud
203 responses become weaker and weaker as DMS emission increases from zero (*DMSZero*) to low (*DMSLow*) and reference
204 (*DMSRef*) level over all of the three regions. The most prominent change in cloud response is over the NPO, followed by the
205 NAO and the SO, which is probably due to the higher contribution of shipping emission to the total sulfur dioxide and sulfate
206 aerosols over the NPO than the NAO and the SO (Figure 2b and 2e). The removal of DMS emission (*DMSZero*) has a much
207 stronger influence on cloud response to shipping emission than reducing DMS emission by half (*DMSLow*), indicating a strong
208 non-linear competing effect for CCN between DMS and shipping emission.

209 3.4 CRE of DMS under various shipping emissions

210 Similar to DMS emissions' impacts on the ISE-induced CRE and cloud properties, ISE could also influence the DMS
211 emission-induced CRE and cloud properties. Generally, stronger cooling net CRE (-7.518 vs. -5.611 W m^{-2}) induced by DMS
212 emissions are seen when shipping emissions are ignored, particularly in areas of intense shipping tracks, such as over the NPO
213 and the NAO (Figure 9). Such a net cooling CRE is mainly the result of SW CRE. Stronger cooling CRE is associated with
214 larger increases in liquid and total CWP (Figure S3) and column-integrated CDNC (Figure S4) in simulations without shipping
215 emissions than those with shipping emissions.

216 It is worth pointing out that DMS emissions have significant warming CRE at LW, particularly over mid- and high-
217 latitude regions in the Southern Hemisphere and high-latitude regions in the Northern Hemisphere regardless of the presence of
218 shipping emissions (Figure 9). Such a warming CRE could be attributed to increases in total cloud area fraction, which is further
219 attributed to increases in the middle and low cloud area fraction in the high-latitude regions in both hemispheres (Figure S5). Our
220 results indicate that DMS is a significant source to CCN in the extremely clean polar regions in both hemispheres.

221 The area-averaged cloud responses over the SO, the NPO, and the NAO, to DMS emissions at different shipping
222 emission levels are shown in Figure 10. Cloud responses to DMS are stronger over the SO than over the NPO and the NAO
223 regardless of the presence of shipping emissions due to the fact that DMS and shipping emissions respectively dominate the
224 sulfur concentrations over the SO, and the NPO and the NAO (Figure 2). Moreover, cloud responses to DMS emissions become
225 much stronger over all of the three oceanic regions when shipping emissions have been removed. However, such changes in



226 cloud responses to DMS due to removal of shipping emissions (i.e., the slopes of the curves) are stronger over the NPO and the
227 NAO than over the SO, which is caused by very limited shipping emissions over the SO. These results again indicate a strong
228 non-linear competing effect for CCN between DMS and shipping emission.

229 3.5 Impacts of choice of aerosol module on the results

230 Besides the impacts of various ISE regulations and DMS emissions on the ISE-induced CRE, various assumptions
231 about the aerosol mixing states could also have an impact. Figure 11 shows the same results as Figure 6 but using MAM3 aerosol
232 module instead of MARC. At the reference level of DMS emissions (DMS_{Ref}), the ISE-induced CRE are generally stronger in
233 MAM3 (SW: -0.319 , LW: $+0.064$, and Net: -0.255 W m^{-2} ; Figure 11) than in MARC (SW: -0.218 , LW: $+0.065$, net: -0.153 W
234 m^{-2} ; Figure 6). More areas with significant cooling CRE are simulated in MAM3 than in MARC, particularly in the Atlantic
235 Ocean, West Pacific Ocean, and North Indian Ocean. At the low level of DMS emissions (DMS_{Low}), both the global averages
236 and spatial patterns of the CRE in MAM3 are very similar to those in MARC. The two aerosol modules show the biggest
237 differences in CRE when DMS emissions are excluded (DMS_{Zero}). MARC simulates strong ISE-induced CRE over tropical
238 regions and the subtropical and mid-latitude areas of the SO, while MAM3 gives no significant CRE over these regions.
239 Generally, the ISE-induced CRE is stronger in MARC than in MAM3 when DMS emissions are excluded. The associated
240 changes in CDNC and CWP due to ISE illustrates similar patterns to changes in CRE (Figures S6 and S7). A possible reason for
241 such differences is the various mixing assumptions about sulfate and sea salt aerosols in MARC (external mixing) versus in
242 MAM3 (internal mixing) and warrants further studies.

243 By comparing Figure 8 with Figure 12 we also observe significantly different impacts of DMS emissions on cloud
244 response to shipping emissions (i.e., the slopes of these curves). MAM3 simulates a weaker impact of DMS emissions on cloud
245 response to shipping emissions than MARC, indicating a weaker non-linear competing effect for CCN between DMS and
246 shipping emissions in MAM3 than MARC.

247 4 Conclusions and Discussion

248 Aerosols from ISE could exert significant cooling on the Earth's climate system through aerosol–cloud and aerosol–
249 radiation interactions. To reduce the pollution and climatic effects from this emission source, the IMO set various emission caps
250 on sulfur content of marine fuel oil to be implemented in the future. Using a state-of-the-art climate model, we find that the
251 newly proposed more stringent emission regulations of shipping emissions can effectively reduce the ISE-induced CRE. As
252 demonstrated in our results, reducing sulfur contents from 3.5% to 2.7% and 0.5% could reduce both DRE (from -51.4 to -36.7
253 and -3.9 mW m^{-2}) and CRE (from -0.179 to -0.153 and -0.001 W m^{-2}) due to ISE, respectively. Although the ISE-induced
254 CRE would be insignificant on a global scale if sulfur contents of ship fuels were reduced to 0.5%, over some regions significant
255 CRE can still be detected—e.g., high latitude regions of the eastern Pacific Ocean. Therefore, implementation of cleaner fuels in
256 shipping sector, such as natural gas, could be a potential solution for completely eliminating sulfate-induced CRE.

257 More importantly, we find that the magnitude and regional spatial pattern of the ISE-induced CRE are highly sensitive
258 to natural DMS emissions. With DMS emissions reducing from 18.2 to 9.1 Tg S yr^{-1} and zero, the ISE-induced net CRE changes
259 from -0.153 to -0.384 and -2.182 W m^{-2} , respectively. On the other hand, the DMS-induced net CRE changes from -5.611 to
260 -7.518 W m^{-2} when shipping emissions at the reference level are removed in the simulations. It is worth noting that DMS is a
261 significant source to CCN in the extremely clean polar regions in both hemispheres. The strong interactions of CRE between
262 DMS and shipping emissions can be attributed to the nonlinearity in the responses of cloud processes to aerosols, particularly the



263 aerosol activation parameterizations (Abdul-Razzak et al., 1998). In a relatively clean environment, activated aerosol number
264 concentration increases as ambient aerosol number concentration increases until reaching a peak at a specific aerosol number
265 concentration, after which it decreases as ambient aerosol number concentration increases unless ambient vapor concentration is
266 drastically increased. In other words, the fraction of activated aerosols decreases as ambient aerosol concentration increases
267 (Figure S8). From the perspective of simulation, this nonlinearity in aerosol activation strongly suggests a reevaluation of CRE
268 induced by shipping and DMS emissions. From the perspective of field measurements of aerosol–cloud relationships, it warrants
269 careful attention when selecting measurement locations—shipping emissions-related measurements should be collected along
270 intense shipping tracks while in areas with as little DMS emissions as possible to avoid contamination from DMS, and vice
271 versa. Moreover, locations containing both shipping and DMS emissions should also be identified and sampled, in order to
272 investigate non-linear interactions between the emissions.

273 Finally, we find that two different aerosol schemes, with different representations of aerosol mixing state, could produce
274 a large difference (about 67%) in the ISE-induced global CRE. Generally, MARC aerosol module shows stronger nonlinear
275 cloud response to DMS and shipping emissions than MAM3. Overall, numerical studies on the uncertainties in the shipping
276 emission-induced CRE due to various ISE regulations, aerosol interactions, and aerosol mixing states can provide useful
277 information for policy makers and have implications for future projections of anthropogenic climate change.

278 Besides the above-mentioned contributors to the uncertainty in estimating the CRE induced by shipping emissions,
279 spatial resolution of the model is another significant source of this uncertainty. Possner et al. (2016) found that the ship-induced
280 shortwave CRE could increase by a factor of two as model spatial resolution decreases from 1 km to 50 km. With higher spatial
281 resolution, models can resolve fine-scale dynamical processes and feedbacks, such as interaction between aerosol and cumulus
282 clouds (Malavelle et al., 2017). Though model resolution-induced uncertainty is not the focus of this study, it should be taken
283 into account when interpreting the spread of shipping-induced CRE in studies of multi-model comparison.

284 Though we employed a state-of-the-art climate model in this study, it is not without caveats, given that neither MARC
285 nor MAM (including both MAM3 and MAM7 in CAM5) aerosol modules treat nitrate aerosols because of the high
286 computational expense for related aerosol-gaseous chemistry and aerosol thermodynamics calculations (Liu et al., 2012). Lack of
287 treating nitrate aerosols could result in uncertainties in our results based on the fact that both mass of nitrate aerosols emitted
288 from international shipping (e.g., Righi et al., 2011) and their hygroscopicity values (e.g., Kawecki and Steiner, 2018) are very
289 similar to those of sulfate aerosols, and thus nitrate aerosols could have non-negligible competing effects on CRE with sulfate
290 aerosols. Despite that some of the results from this study could be used to qualitatively project the potential outcome, a
291 quantitative assessment should be facilitated to address this topic with an improved model.

292 Acknowledgments

293 This study is supported by Concawe, whose mission is to conduct research on environmental issues relevant to the oil refining
294 industry. This research is also partially supported by the U.S. National Science Foundation (AGS-1339264), the U.S. Department
295 of Energy (DE-FG02-94ER61937), and the National Research Foundation (NRF) of Singapore under its Campus for Research
296 Excellence and Technological Enterprise programme. The Center for Environmental Sensing and Modeling (CENSAM) is an
297 interdisciplinary research group of the Singapore-MIT Alliance for Research and Technology (SMART). The CESM project is
298 supported by the National Science Foundation and the Office of Science (BER) of the U.S. Department of Energy. We would
299 like to acknowledge high-performance computing support from Yellowstone (ark:/85065/d7wd3xhc) provided by NCAR's
300 Computational and Information Systems Laboratory, sponsored by the National Science Foundation.

**301 Conflict of interest**

302 The authors declare no competing interests.

303 Data and code availability

304 The MARC source code is available via https://github.mit.edu/marc/marc_cesm/ and also archived with DOI
305 10.5281/zenodo.1117370, along with documentation on how to install and run the model. The commit 23e08fe was used in this
306 study. All the analysis code and model output data analyzed are available via
307 <https://drive.google.com/drive/folders/1GHjrpvO06mzC8iFyTOEif0PRiI56cReV?usp=sharing>.

308 References

- 309 Abdul-Razzak, H., Ghan, S. J., and Rivera-Carpio, C.: A parameterization of aerosol activation - 1. Single aerosol type, J
310 Geophys Res-Atmos, 103, 6123-6131, 1998.
- 311 Albani, S., Mahowald, N. M., Perry, A. T., Scanza, R. A., Zender, C. S., Heavens, N. G., Maggi, V., Kok, J. F., and Otto-
312 Bliesner, B. L.: Improved dust representation in the Community Atmosphere Model, J Adv Model Earth Sy, 6, 541-570,
313 2014.
- 314 Boucher, O., Moulin, C., Belviso, S., Aumont, O., Bopp, L., Cosme, E., von Kuhlmann, R., Lawrence, M. G., Pham, M., Reddy,
315 M. S., Sciare, J., and Venkataraman, C.: DMS atmospheric concentrations and sulphate aerosol indirect radiative
316 forcing: a sensitivity study to the DMS source representation and oxidation, Atmos Chem Phys, 3, 49-65, 2003.
- 317 Boucher, O., Randall, D., Artaxo, P., Bretherton, C., Feingold, G., Forster, P., Kerminen, V.-M., Kondo, Y., Liao, H., Lohmann,
318 U., Rasch, P., Satheesh, S. K., Sherwood, S., Stevens, B., and Zhang, X. Y.: Clouds and Aerosols, in: Climate Change
319 2013: The Physical Science Basis. Contribution of Working Group I to the Fifth Assessment Report of the
320 Intergovernmental Panel on Climate Change, edited by: Stocker, T. F., Qin, D., Plattner, G.-K., Tignor, M., Allen, S.
321 K., Boschung, J., Nauels, A., Xia, Y., Bex, V., and Midgley, P. M., Cambridge University Press, Cambridge, United
322 Kingdom and New York, NY, USA, 571-658, 2013.
- 323 Capaldo, K., Corbett, J. J., Kasibhatla, P., Fischbeck, P., and Pandis, S. N.: Effects of ship emissions on sulphur cycling and
324 radiative climate forcing over the ocean, Nature, 400, 743-746, 1999.
- 325 Corbett, J. J., and Koehler, H. W.: Updated emissions from ocean shipping, J Geophys Res-Atmos, 108, 2003.
- 326 Corbett, J. J., Winebrake, J. J., Green, E. H., Kasibhatla, P., Eyring, V., and Lauer, A.: Mortality from ship emissions: A global
327 assessment, Environ Sci Technol, 41, 8512-8518, 2007.
- 328 Dentener, F., Kinne, S., Bond, T., Boucher, O., Cofala, J., Generoso, S., Ginoux, P., Gong, S., Hoelzemann, J. J., Ito, A., Marelli,
329 L., Penner, J. E., Putaud, J. P., Textor, C., Schulz, M., van der Werf, G. R., and Wilson, J.: Emissions of primary aerosol
330 and precursor gases in the years 2000 and 1750 prescribed data-sets for AeroCom, Atmos Chem Phys, 6, 4321-4344,
331 2006.
- 332 Devasthale, A., Kruger, O., and Grassl, H.: Impact of ship emissions on cloud properties over coastal areas, Geophys Res Lett,
333 33, 2006.
- 334 Endresen, O., Sorgard, E., Sundet, J. K., Dalsoren, S. B., Isaksen, I. S. A., Berglen, T. F., and Gravir, G.: Emission from
335 international sea transportation and environmental impact, J Geophys Res-Atmos, 108, 2003.
- 336 Endresen, O., Bakke, J., Sorgard, E., Berglen, T. F., and Holmvang, P.: Improved modelling of ship SO₂ emissions - a fuel-
337 based approach, Atmos Environ, 39, 3621-3628, 2005.
- 338 Eyring, V., Isaksen, I. S. A., Bernsten, T., Collins, W. J., Corbett, J. J., Endresen, O., Grainger, R. G., Moldanova, J., Schlager,
339 H., and Stevenson, D. S.: Transport impacts on atmosphere and climate: Shipping, Atmos Environ, 44, 4735-4771,
340 2010.
- 341 Gettelman, A., Liu, X., Ghan, S. J., Morrison, H., Park, S., Conley, A. J., Klein, S. A., Boyle, J., Mitchell, D. L., and Li, J. L. F.:
342 Global simulations of ice nucleation and ice supersaturation with an improved cloud scheme in the Community
343 Atmosphere Model, J Geophys Res-Atmos, 115, 2010.
- 344 Grandey, B. S., and Wang, C.: Enhanced marine sulphur emissions offset global warming and impact rainfall, Scientific Reports,
345 5, 2015.
- 346 Grandey, B. S., Rothenberg, D., Avramov, A., Jin, Q., Lee, H.-H., Liu, X., Lu, Z., Albani, S., and Wang, C.: Effective radiative
347 forcing in the aerosol-climate model CAM5.3-MARC-ARG, arXiv:1804.06158, 2018.
- 348 Gunson, J. R., Spall, S. A., Anderson, T. R., Jones, A., Totterdell, I. J., and Woodage, M. J.: Climate sensitivity to ocean
349 dimethylsulphide emissions, Geophys Res Lett, 33, 2006.
- 350 International Maritime Organization: IMO sets 2020 date for ships to comply with low sulphur fuel oil requirement, 2016.



- 351 Kawecki, S., and Steiner, A. L.: The Influence of Aerosol Hygroscopicity on Precipitation Intensity During a Mesoscale
352 Convective Event, *J Geophys Res-Atmos*, 123, 424-442, 2018.
- 353 Kim, D., Wang, C., Ekman, A. M. L., Barth, M. C., and Rasch, P. J.: Distribution and direct radiative forcing of carbonaceous
354 and sulfate aerosols in an interactive size-resolving aerosol-climate model, *J Geophys Res-Atmos*, 113, 2008.
- 355 Kim, D., Wang, C., Ekman, A. M. L., Barth, M. C., and Lee, D. I.: The responses of cloudiness to the direct radiative effect of
356 sulfate and carbonaceous aerosols, *J Geophys Res-Atmos*, 119, 1172-1185, 2014.
- 357 Klein, S. A., and Hartmann, D. L.: The Seasonal Cycle of Low Stratiform Clouds, *Journal of Climate*, 6, 1587-1606, 1993.
- 358 Klimont, Z., Smith, S. J., and Cofala, J.: The last decade of global anthropogenic sulfur dioxide: 2000-2011 emissions, *Environ*
359 *Res Lett*, 8, 2013.
- 360 Lauer, A., Eyring, V., Hendricks, J., Jockel, P., and Lohmann, U.: Global model simulations of the impact of ocean-going ships
361 on aerosols, clouds, and the radiation budget, *Atmos Chem Phys*, 7, 5061-5079, 2007.
- 362 Lauer, A., Eyring, V., Corbett, J. J., Wang, C. F., and Winebrake, J. J.: Assessment of Near-Future Policy Instruments for
363 Oceangoing Shipping: Impact on Atmospheric Aerosol Burdens and the Earth's Radiation Budget, *Environ Sci Technol*,
364 43, 5592-5598, 2009.
- 365 Liu, X., Easter, R. C., Ghan, S. J., Zaveri, R., Rasch, P., Shi, X., Lamarque, J. F., Gettelman, A., Morrison, H., Vitt, F., Conley,
366 A., Park, S., Neale, R., Hannay, C., Ekman, A. M. L., Hess, P., Mahowald, N., Collins, W., Iacono, M. J., Bretherton, C.
367 S., Flanner, M. G., and Mitchell, D.: Toward a minimal representation of aerosols in climate models: description and
368 evaluation in the Community Atmosphere Model CAM5, *Geosci Model Dev*, 5, 709-739, 2012.
- 369 Mahajan, A. S., Fadnavis, S., Thomas, M. A., Pozzoli, L., Gupta, S., Royer, S. J., Saiz-Lopez, A., and Simo, R.: Quantifying the
370 impacts of an updated global dimethyl sulfide climatology on cloud microphysics and aerosol radiative forcing, *J*
371 *Geophys Res-Atmos*, 120, 2524-2536, 2015.
- 372 Mahowald, N. M., Muhs, D. R., Levis, S., Rasch, P. J., Yoshioka, M., Zender, C. S., and Luo, C.: Change in atmospheric mineral
373 aerosols in response to climate: Last glacial period, preindustrial, modern, and doubled carbon dioxide climates, *J*
374 *Geophys Res-Atmos*, 111, 2006.
- 375 Malavelle, F. F., Haywood, J. M., Jones, A., Gettelman, A., Clarisse, L., Bauduin, S., Allan, R. P., Karset, I. H. H., Kristjansson,
376 J. E., Oreopoulos, L., Cho, N., Lee, D., Bellouin, N., Boucher, O., Grosvenor, D. P., Carslaw, K. S., Dhomse, S., Mann,
377 G. W., Schmidt, A., Coe, H., Hartley, M. E., Dalvi, M., Hill, A. A., Johnson, B. T., Johnson, C. E., Knight, J. R.,
378 O'Connor, F. M., Partridge, D. G., Stier, P., Myhre, G., Platnick, S., Stephens, G. L., Takahashi, H., and Thordarson, T.:
379 Strong constraints on aerosol-cloud interactions from volcanic eruptions, *Nature*, 546, 485-491, 10.1038/nature22974,
380 2017.
- 381 McCoy, D. T., Burrows, S. M. W., Robert, Grosvenor, D. P., Elliott, S. M., Ma, P.-L., Rasch, P. J., and Hartmann, D. L.:
382 Natural aerosols explain seasonal and spatial patterns of Southern Ocean cloud albedo, 1, 10.1126/sciadv.1500157,
383 2015.
- 384 Morrison, H., and Gettelman, A.: A new two-moment bulk stratiform cloud microphysics scheme in the community atmosphere
385 model, version 3 (CAM3). Part I: Description and numerical tests, *Journal of Climate*, 21, 3642-3659, 2008.
- 386 Neubauer, D., Lohmann, U., Hoose, C., and Frontoso, M. G.: Impact of the representation of marine stratocumulus clouds on the
387 anthropogenic aerosol effect, *Atmos Chem Phys*, 14, 11997-12022, 2014.
- 388 Notteboom, T.: The impact of low sulphur fuel requirements in shipping on the competitiveness of ro-ro shipping in Northern
389 Europe, *WMU Journal of Maritime Affairs*, 10, 63-95, 10.1007/s13437-010-0001-7, 2010.
- 390 Pandis, S. N., Russell, L. M., and Seinfeld, J. H.: The Relationship between Dms Flux and Ccn Concentration in Remote Marine
391 Regions, *J Geophys Res-Atmos*, 99, 16945-16957, 1994.
- 392 Partanen, A. I., Laakso, A., Schmidt, A., Kokkola, H., Kuokkanen, T., Pietikainen, J. P., Kerminen, V. M., Lehtinen, K. E. J.,
393 Laakso, L., and Korhonen, H.: Climate and air quality trade-offs in altering ship fuel sulfur content, *Atmos Chem Phys*,
394 13, 12059-12071, 2013.
- 395 Peters, K., Stier, P., Quaas, J., and Grassl, H.: Aerosol indirect effects from shipping emissions: sensitivity studies with the
396 global aerosol-climate model ECHAM-HAM, *Atmos Chem Phys*, 12, 5985-6007, 2012.
- 397 Possner, A., Zubler, E., Lohmann, U., and Schär, C.: The resolution dependence of cloud effects and ship-induced aerosol-cloud
398 interactions in marine stratocumulus, *Journal of Geophysical Research: Atmospheres*, 121, 4810-4829,
399 10.1002/2015jd024685, 2016.
- 400 Quinn, P. K., Bates, T. S., Covert, D. S., Ramsey-Bell, D. C., and McInnes, L.: Dimethylsulphide: Oceans, Atmosphere and
401 Climate, in: *Air Pollution Research Reports*, 1 ed., edited by: Restelli, G., and Angeletti, G., 43, Springer Netherlands,
402 400, 1993.
- 403 Righi, M., Klinger, C., Eyring, V., Hendricks, J., Lauer, A., and Petzold, A.: Climate Impact of Biofuels in Shipping: Global
404 Model Studies of the Aerosol Indirect Effect, *Environ Sci Technol*, 45, 3519-3525, 2011.
- 405 Rothenberg, D., and Wang, C.: Metamodeling of Droplet Activation for Global Climate Models, *J Atmos Sci*, 73, 1255-1272,
406 2016.
- 407 Rothenberg, D., Avramov, A., and Wang, C.: On the representation of aerosol activation and its influence on model-derived
408 estimates of the aerosol indirect effect, *Atmospheric Chemistry and Physics Discussions*, 1-35, 10.5194/acp-2017-680,
409 2017.



- 410 Rothenberg, D., and Wang, C.: An aerosol activation metamodel of v1.2.0 of the pyrcel cloud parcel model: development and
411 offline assessment for use in an aerosol-climate model, *Geosci Model Dev*, 10, 1817-1833, 2017.
- 412 Russell, L. M., Pandis, S. N., and Seinfeld, J. H.: Aerosol Production and Growth in the Marine Boundary-Layer, *J Geophys*
413 *Res-Atmos*, 99, 20989-21003, 1994.
- 414 Scanza, R. A., Mahowald, N., Ghan, S., Zender, C. S., Kok, J. F., Liu, X., Zhang, Y., and Albani, S.: Modeling dust as
415 component minerals in the Community Atmosphere Model: development of framework and impact on radiative forcing,
416 *Atmos Chem Phys*, 15, 537-561, 2015.
- 417 Schreier, M., Mannstein, H., Eyring, V., and Bovensmann, H.: Global ship track distribution and radiative forcing from 1 year of
418 AATSR data, *Geophys Res Lett*, 34, 2007.
- 419 Tesdal, J. E., Christian, J. R., Monahan, A. H., and von Salzen, K.: Sensitivity of modelled sulfate aerosol and its radiative effect
420 on climate to ocean DMS concentration and air-sea flux, *Atmos Chem Phys*, 16, 10847-10864, 2016.
- 421 Thomas, M. A., Suntharalingam, P., Pozzoli, L., Rast, S., Devasthale, A., Kloster, S., Feichter, J., and Lenton, T. M.:
422 Quantification of DMS aerosol-cloud-climate interactions using the ECHAM5-HAMMOZ model in a current climate
423 scenario, *Atmos Chem Phys*, 10, 7425-7438, 2010.
- 424 Thomas, M. A., Suntharalingam, P., Pozzoli, L., Devasthale, A., Kloster, S., Rast, S., Feichter, J., and Lenton, T. M.: Rate of
425 non-linearity in DMS aerosol-cloud-climate interactions, *Atmos Chem Phys*, 11, 11175-11183, 2011.
- 426 Warren, S. G., Hahn, C. J., London, J., Chervin, R. M., and Jenne, R. L.: Global Distribution of Total Cloud Cover and Cloud
427 Type Amounts Over Ocean, NCAR Technical Note NCAR/TN-273+STR, doi:10.5065/D6GH9FXB, 1988.
- 428 Winebrake, J. J., Corbett, J. J., Green, E. H., Lauer, A., and Eyring, V.: Mitigating the Health Impacts of Pollution from
429 Oceangoing Shipping: An Assessment of Low-Sulfur Fuel Mandates, *Environ Sci Technol*, 43, 4776-4782, 2009.
- 430

431

432

433

434

435

436

437

438

439

440

441

442

443

444

445

446

447

448

449

450

451

452

453

454

455

456

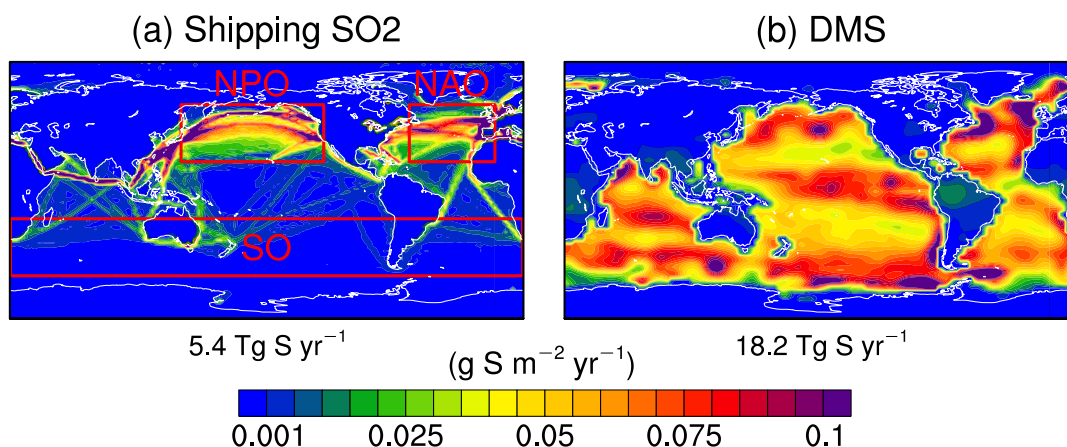


457 **Table 1. Summary of experiments.**

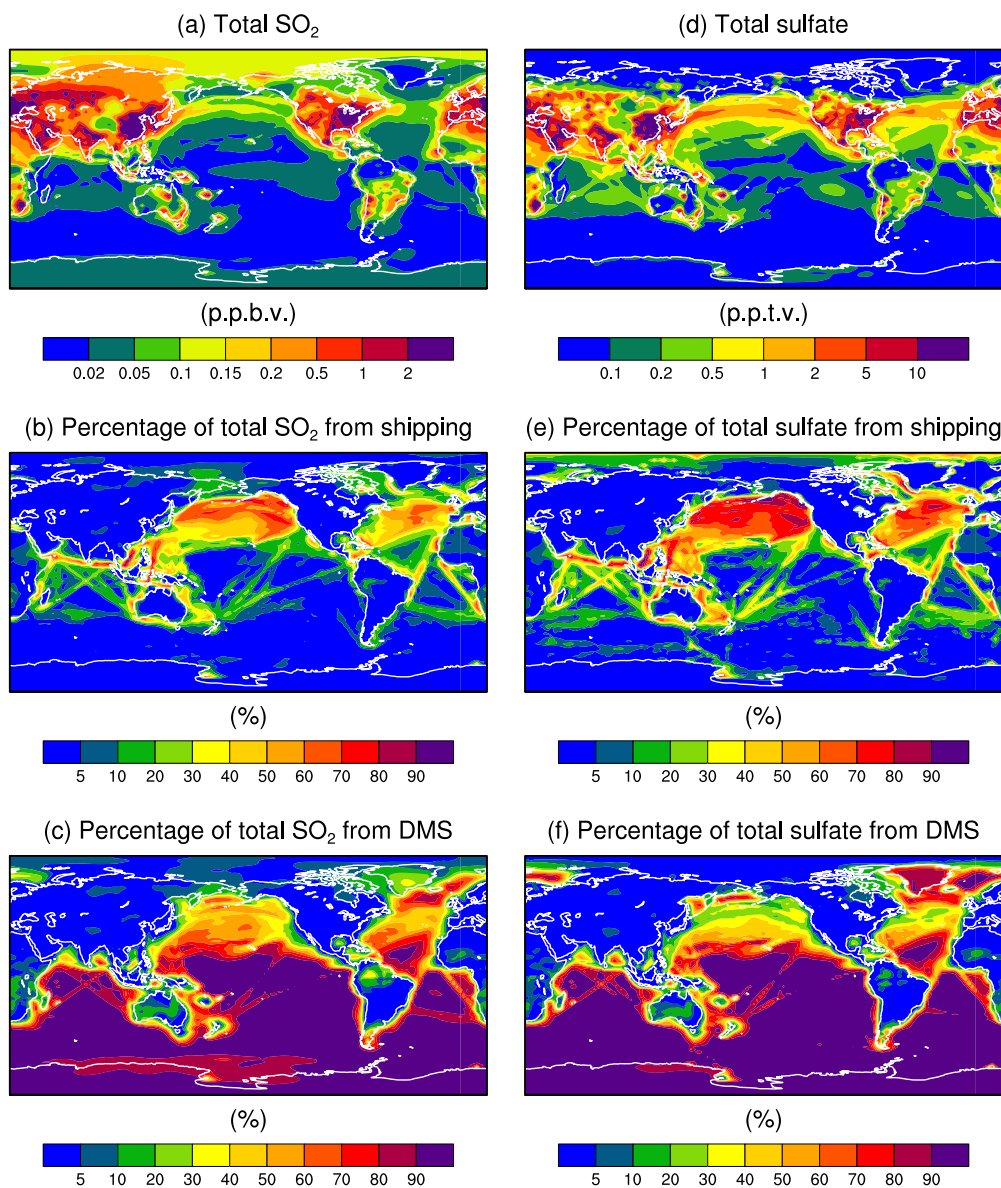
Aerosol Modules	Experiments	DMS emissions	Ship emissions	Description
MARC	Shipping	<i>DMSRef</i>	<i>ShipZero</i>	DMS emission (Tg S yr^{-1}): DMSZero: 0 DMSLow: 9.1 DMSRef: 18.2 Ship emission (Tg S yr^{-1}): ShipZero: 0 ShipLow: 1.0 (0.5%) ShipRef: 5.4 (2.7%) ShipHigh: 7.0 (3.5%)
			<i>ShipLow</i>	
			<i>ShipRef</i>	
			<i>ShipHigh</i>	
	DMS	<i>DMSZero</i>	<i>ShipZero</i>	
			<i>ShipRef</i>	
<i>DMSLow</i>	<i>ShipZero</i>			
	<i>ShipRef</i>			
MAM3	DMS	<i>DMSRef</i>	<i>ShipZero</i>	
			<i>ShipRef</i>	
		<i>DMSZero</i>	<i>ShipZero</i>	
			<i>ShipRef</i>	
		<i>DMSLow</i>	<i>ShipZero</i>	
			<i>ShipRef</i>	

458 Notes: in *ShipZero* experiments, emission rates of all gas-phase and aerosol species from shipping emissions are set to zero;
 459 while in *ShipLow*, *ShipRef*, and *ShipHigh* experiments, all shipping emission rates (such as OC and BC) are set to observations
 460 except for emission rates of sulfur compounds (i.e. SO_2 and SO_4) which are modified.

461



462 **Figure 1. Spatial patterns of annual means of sulfur emission ($\text{g S m}^{-2} \text{yr}^{-1}$) from (a) international shipping and (b) natural DMS in the**
 463 **simulation at the reference emission level (i.e., *ShipRef* *DMSRef*). The numbers below each panel are the global total annual emissions.**
 464 **Three regions are selected for further analysis: The North Pacific Ocean (NPO; 20°N – 60°N , 140°E – 240°E), the North Atlantic Ocean**
 465 **(NAO; 20°N – 60°N , 300°E – 360°E), and the Southern Ocean (SO; 20°S – 60°S , 0°E – 360°E).**
 466



467

468

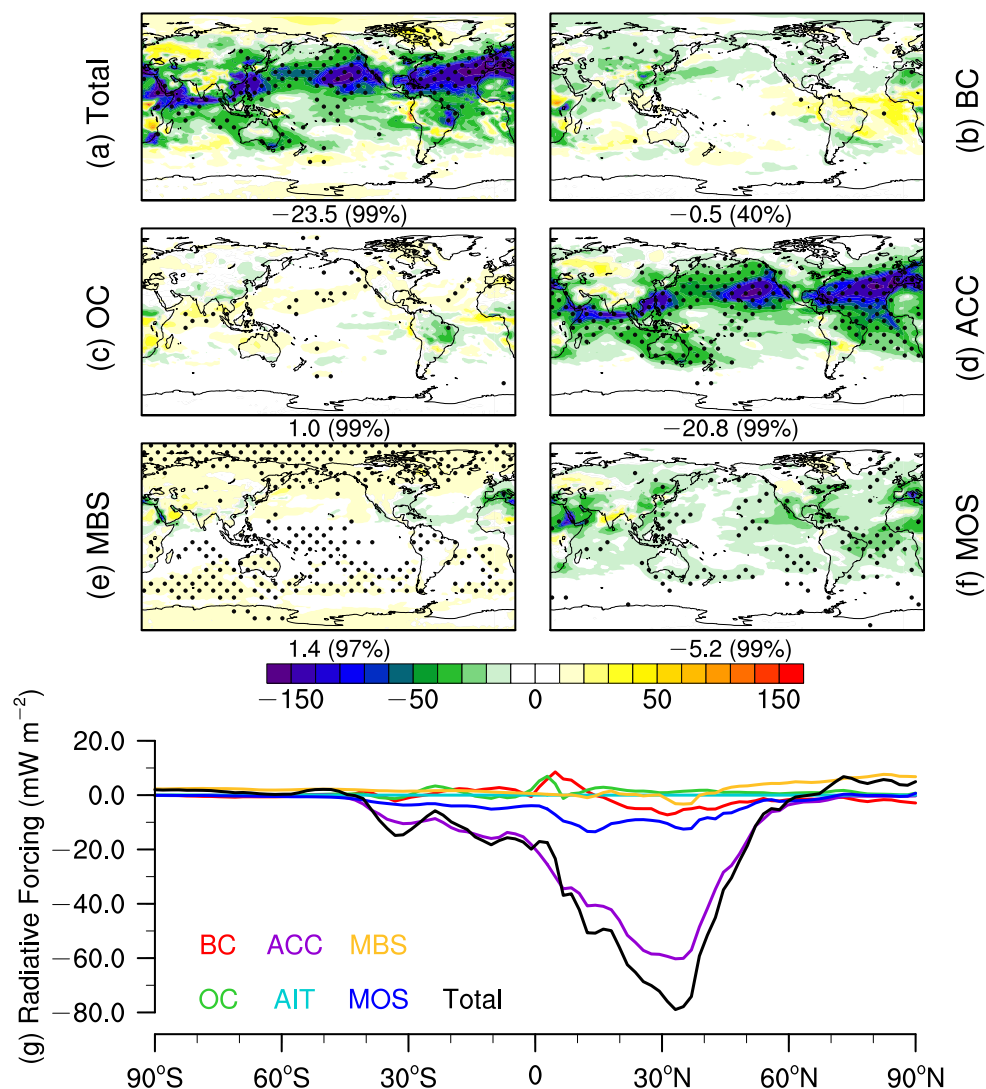
469

470

471

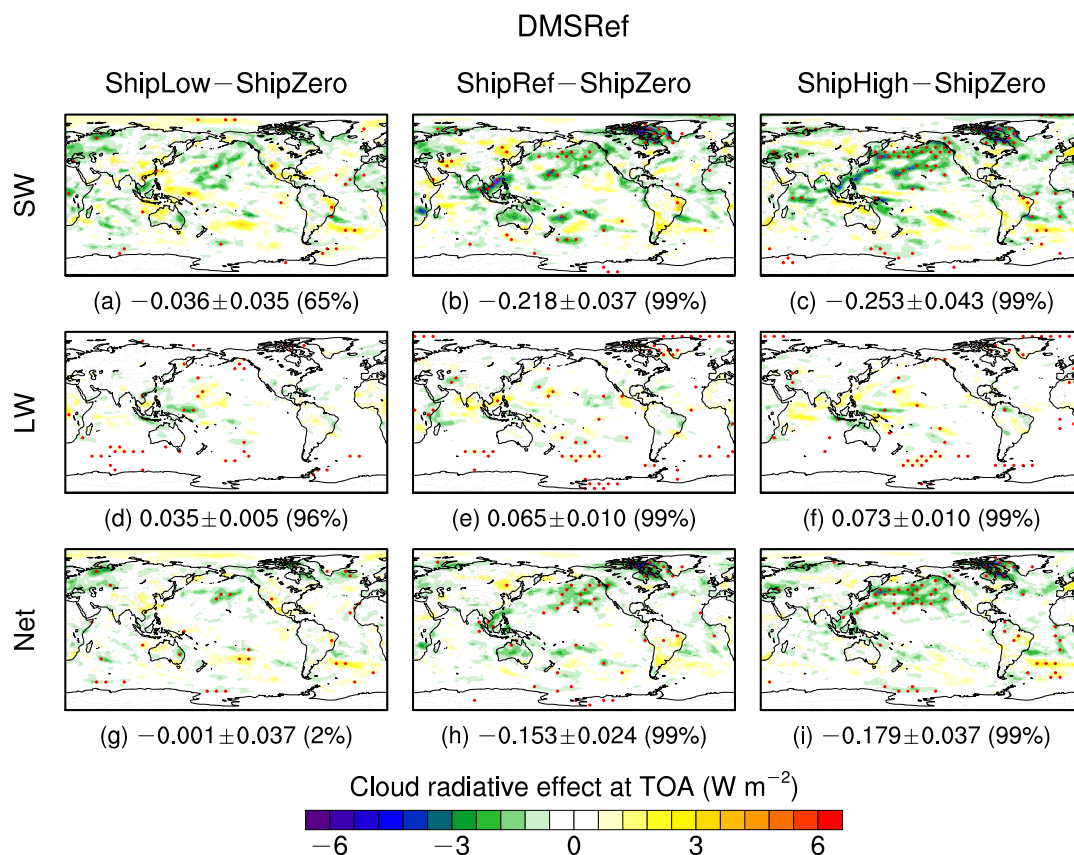
472

Figure 2. Spatial patterns of (a) annual mean concentrations of total SO₂ (units: parts per billion by volume; ppbv), (b) and (c) are respectively the contributions of shipping emission and natural DMS to total SO₂ in the lowest model layer. (d)–(f) are the same as (a)–(c), but for sulfate aerosols. These results are from MARC simulations and calculated as the differences between the simulations with the international shipping and DMS emissions at the reference and zero levels (i.e., *ShipRef_DMSRef* minus *ShipZero_DMSRef* and *ShipRef_DMSRef* minus *ShipRef_DMSZero*).



473

474 Figure 3. Simulated direct radiative effect (DRE; units: mW m^{-2}) of ISE at TOA by MARC. The DRE is calculated as the difference
 475 between simulation results with and without ISE (i.e., *ShipRef_DMSRef* minus *ShipZero_DMSRef*) and averaged over the 30-year
 476 period of simulations at all-sky conditions. Panels (a)–(f) show the spatial patterns of DRE due to ISE with the global mean differences
 477 and the associated significant levels indicated by the numbers below each panel and panel (g) is the meridional variations of zonal
 478 mean DRE for various aerosol types from ISE and their total effects. The expansions of the abbreviations can be found in Section 2.3.
 479 The black dots represent grid points that are statistically significant above the 90% confidence level based on the two-tailed Student's
 480 *t*-test.



481

482 Figure 4. Spatial patterns of MARC simulated cloud radiative effect (CRE; units: W m^{-2}) at TOA of ISE with various shipping
 483 emission levels. The CRE is calculated as the differences of radiation flux at TOA and at all-sky conditions between the simulation
 484 without shipping emissions and three simulations with the same DMS emissions at the reference level but various shipping emission
 485 levels (i.e., low, reference, high) in short-wave (SW), long-wave (LW), and net (SW+LW) and averaged over the 30-year simulation
 486 period. The numbers below each panel are the global means, standard deviation across the 30-year period, and the confidence level.
 487 The red dots represent grid points that are statistically significant above the 90% confidence level based on the two-tailed Student's *t*-
 488 test.

489

490

491

492

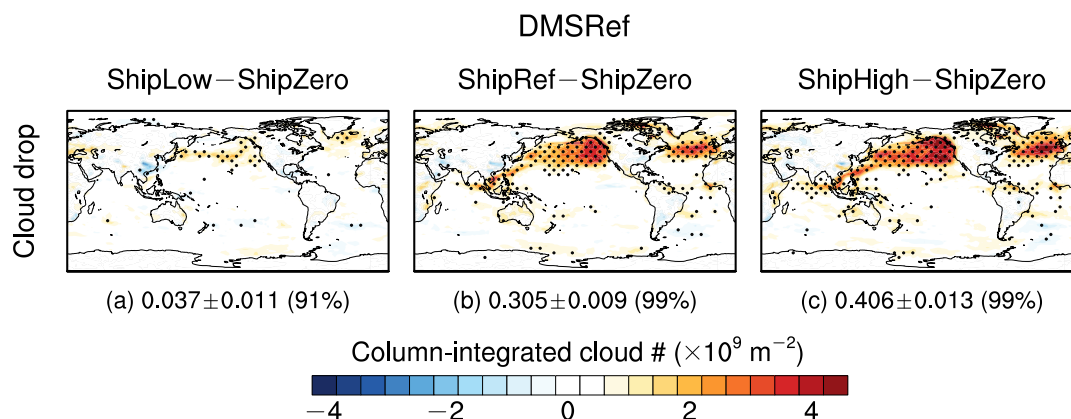
493

494

495

496

497



498

499 **Figure 5. Spatial patterns of MARC simulated column-integrated cloud droplet number concentration ($\times 10^9 \text{ m}^{-2}$) response to**
 500 **international shipping emissions. The responses are calculated as the differences of cloud droplet number integrated through the whole**
 501 **atmospheric columns between the simulation without shipping emissions and three simulations with the reference shipping emission**
 502 **and various DMS emissions (i.e., zero, low, and reference) over the 30-year simulation period. The numbers below each panel are the**
 503 **global means, standard deviation across the 30-year period, and the confidence level. The black dots represent grid points that are**
 504 **statistically significant above the 90% confidence level based on the two-tailed Student's *t*-test.**

505

506

507

508

509

510

511

512

513

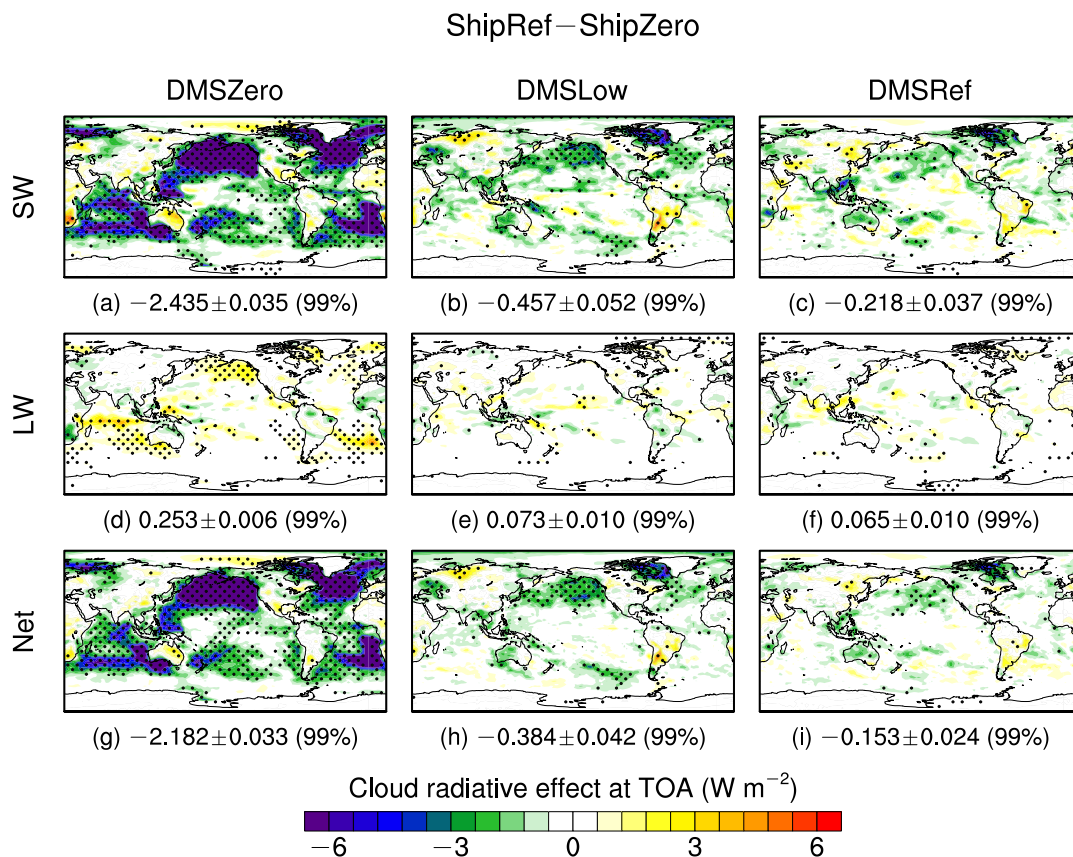
514

515

516

517

518



519

520 Figure 6. Spatial patterns of MARC simulated cloud radiative effect (CRE; units: W m^{-2}) at TOA of ISE at various DMS emission
 521 levels. The CRE is calculated as the differences of radiation flux at TOA and at all-sky conditions between the simulation without
 522 shipping emissions and three simulations with the same shipping emissions at the reference level but various DMS emission levels (i.e.,
 523 zero, low, and reference) in short-wave (SW), long-wave (LW), and net (SW+LW) and averaged over the 30-year simulation period.
 524 The numbers below each panel are the global means, standard deviation across the 30-year period, and the confidence level. The black
 525 dots represent grid points that are statistically significant above the 90% confidence level based on the two-tailed Student's *t*-test.

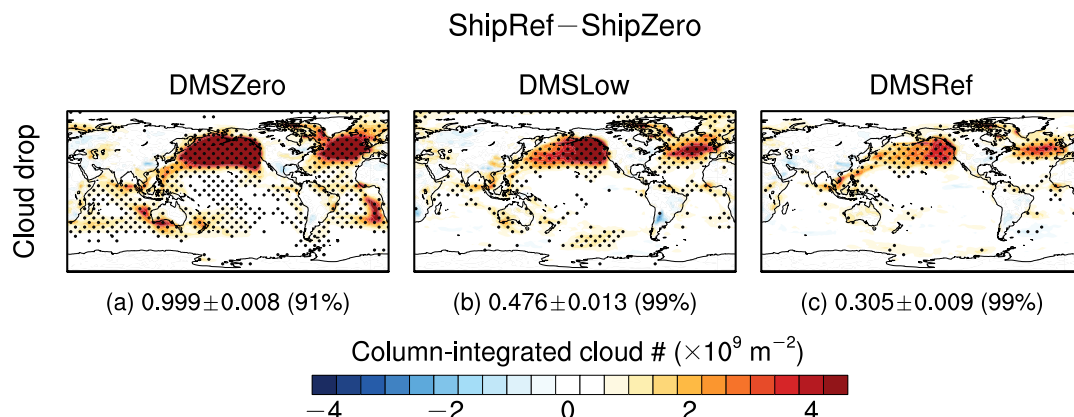
526

527

528

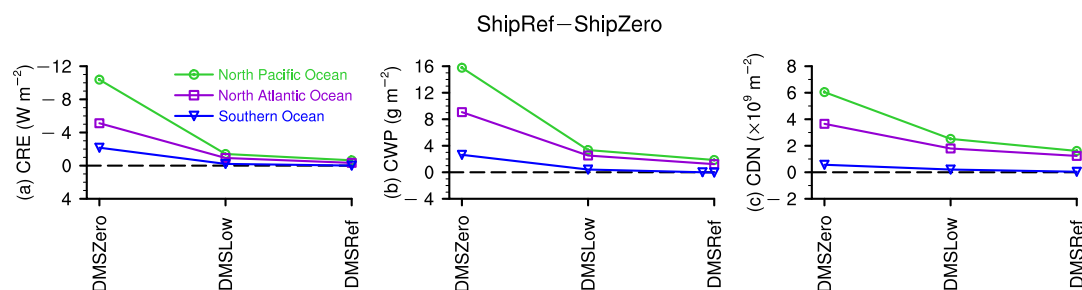
529

530



531

532 **Figure 7.** Spatial patterns of MARC simulated column-integrated cloud droplet number concentration ($\times 10^9 \text{ m}^{-2}$) response to
 533 international shipping emissions. The responses are calculated as the differences of cloud droplet number integrated through the whole
 534 atmospheric columns between the simulation without shipping emissions and three simulations with the reference shipping emission
 535 and various DMS emissions (i.e., zero, low, and reference) over the 30-year simulation period. The numbers below each panel are the
 536 global means, standard deviation across the 30-year period, and the confidence level. The black dots represent grid points that are
 537 statistically significant above the 90% confidence level based on the two-tailed Student's *t*-test.



538

539 **Figure 8.** Impacts of DMS emissions on cloud responses to international shipping emissions. (a) Cloud radiative effects at TOA (W
 540 m^{-2}), (b) column-integrated cloud water path (g m^{-2}), and (c) column-integrated cloud droplet number ($\times 10^9 \text{ m}^{-2}$). The green, purple,
 541 and blue curves respectively represent quantities area-averaged over the North Pacific Ocean (NPO), the North Atlantic Ocean (NAO),
 542 and the Southern Ocean (SO), which are shown as red boxes in Figure 1a. These results are from MARC simulations.

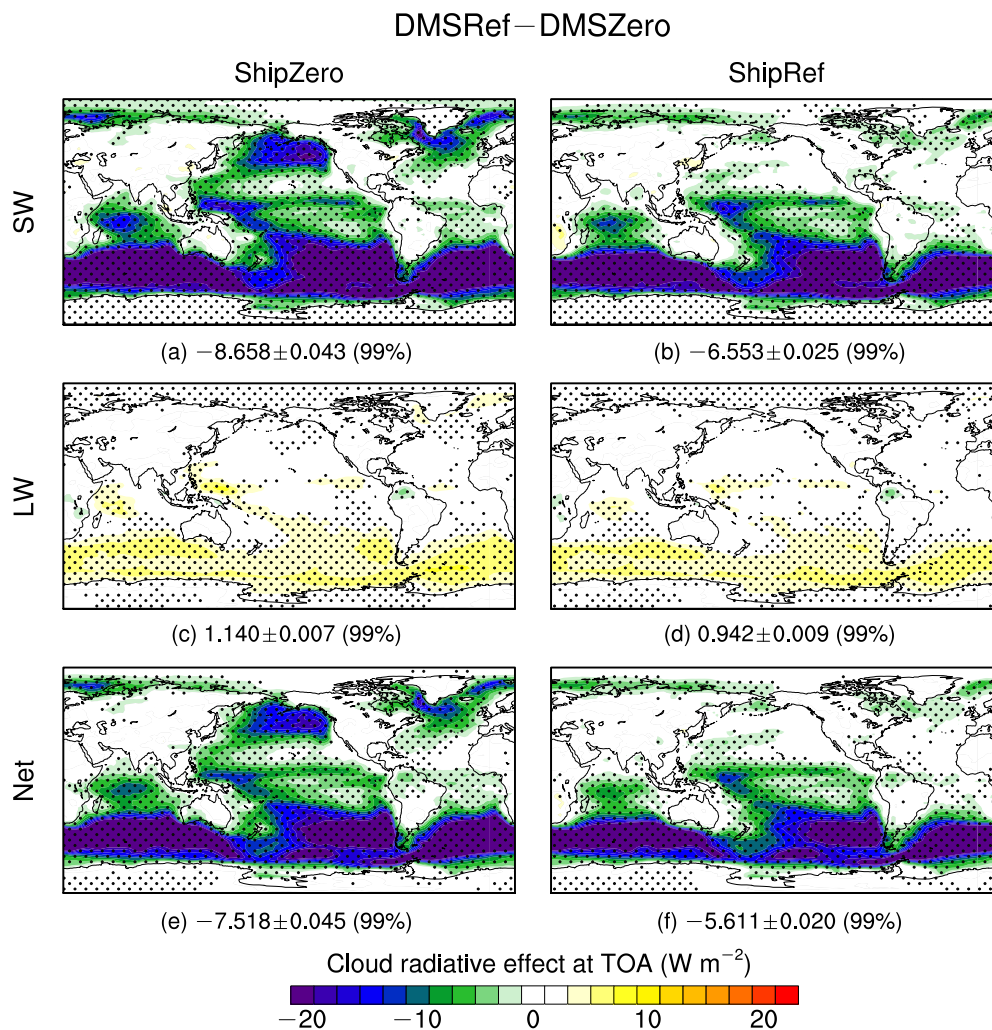
543

544

545

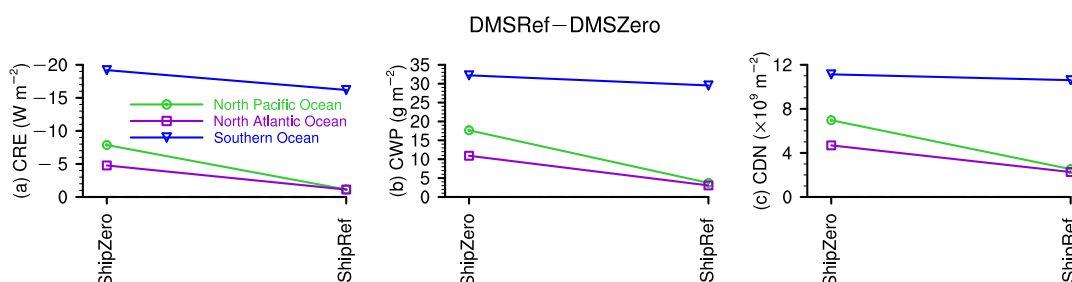
546

547



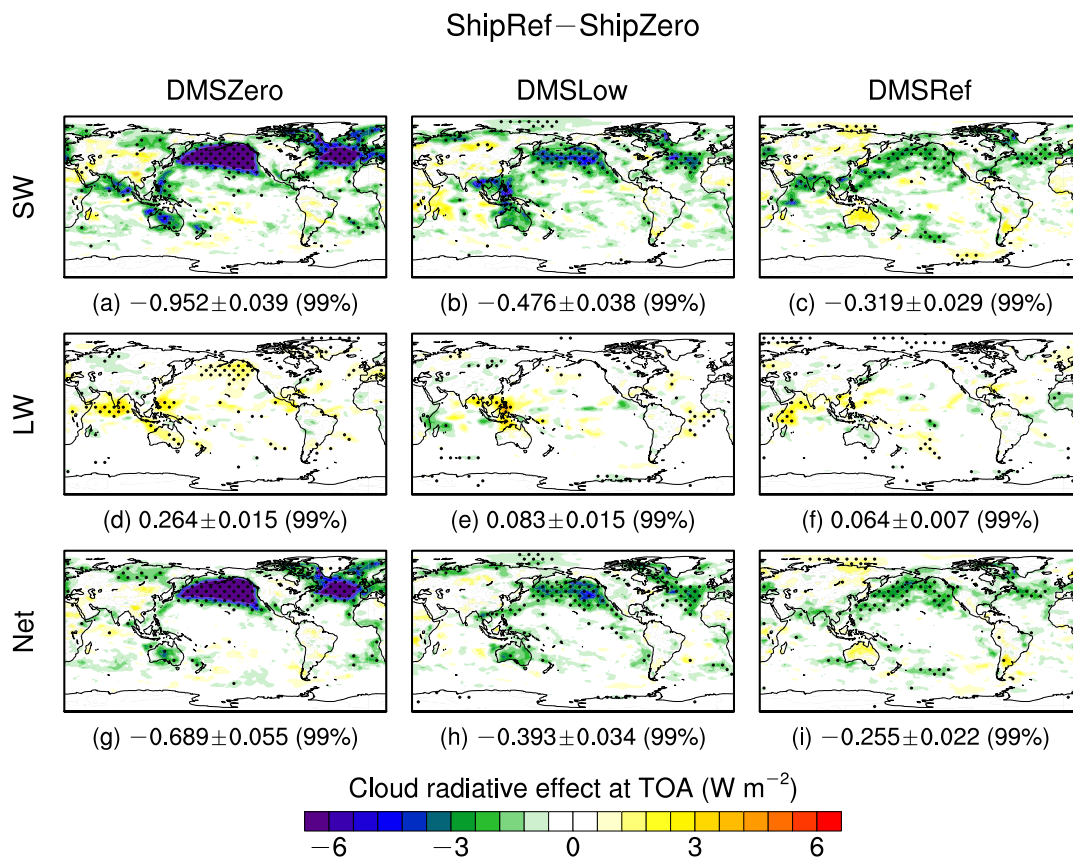
548

549 **Figure 9.** Spatial patterns of MARC simulated cloud radiative effect (units: W m^{-2}) of DMS emissions at various shipping emission
 550 levels. The CRE is calculated as the differences of radiation flux at TOA and at all-sky conditions between the simulation without DMS
 551 emissions and two simulations with the same DMS emissions at the reference level but various shipping emission levels (i.e., zero and
 552 reference) in short-wave (SW), long-wave (LW), and net (SW+LW) and averaged over the 30-year simulation period. The numbers
 553 below each panel are the global means, standard deviation across the 30-year period, and the confidence level. The black dots
 554 represent grid points that are statistically significant above the 90% confidence level based on the two-tailed Student's t -test.



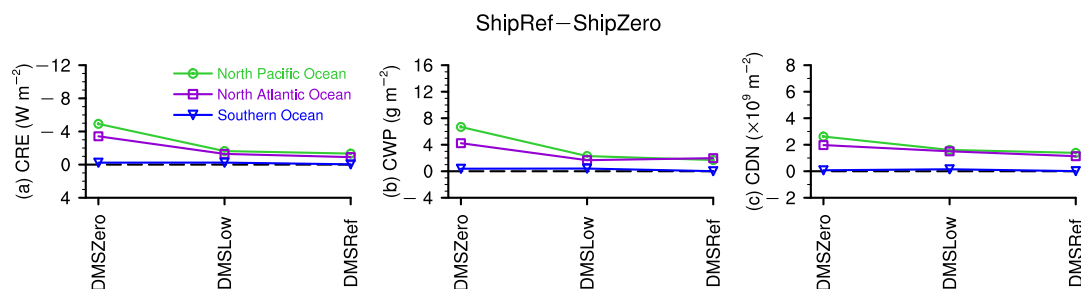
555

556 **Figure 10.** Impacts of ISE on cloud responses to DMS emissions. (a) Cloud radiative effects at TOA (W m^{-2}), (b) column-integrated
 557 cloud water path (g m^{-2}), and (c) column-integrated cloud droplet number ($\times 10^9 \text{ m}^{-2}$). The green, purple, and blue curves respectively
 558 represent quantities area-averaged over the North Pacific Ocean (NPO), the North Atlantic Ocean (NAO), and the Southern Ocean
 559 (SO), which are shown as red boxes in Figure 1a. These results are from MARC simulations.



560

561 Figure 11. Same as Figure 6, but using a different aerosol module, namely MAM3 rather than MARC.



562

563 Figure 12. Same as Figure 8, but using a different aerosol module, namely MAM3 rather than MARC.